Numerical Analysis of Narrow-gap Underfill Flow in the Flip-chip Process Using the Lattice Boltzmann Method

Jung Shin Lee, Sujie Kang, and Daniel Min Woo Rhee
Mechatronics Research, Samsung Electronics
1-1, Samsungjeonja-ro
Hwaseong-si, 18448, Republic of Korea
Ph: +82-10-4623-3386
Email: jrebotco.lee@samsung.com

Abstract

Flip-chip packaging is a first-level interconnect technology, and to predict its melt front of capillary driven underfill analytical models have been made. Using the Analytical models, prediction of the melt front can be efficiently done, however it is difficult to reflect the flow resistance resulting from complex solder bump arrangement. Therefore, 3D numerical analysis is required. In this study, Lattice Boltzmann method (LBM) is used for observing the micro void generation that occurs in a underfill process with a height of several tens of microns. LBM statistically expresses the motion of the molecule, to solve the mass transfer of the microscale. In particular, LBM has strengths in multiphase flow analysis of several microscales that cannot be solved by continuum assumption. In this paper, underfill process of several tens of micro scales, which was not covered in previous 3D numerical analysis studies, was simulated using LBM. The improvement of the new LBM model, which more accurately simulates the resistance due to pressure by considering collisions between air and molten mold molecules, is introduced. With the hydraulic diameter greatly reduced due to the narrow gap, it is observed how the solder bump pitch affects the micro void generation. And it is observed whether the air ventilation could change significantly according to the ambient pressure.

Key words

Underfill encapsulation, Lattice Boltzmann method, Flip-chip packaging, Micro void

I. Introduction

Flip-chip packaging is a first-level interconnect technology that was first developed about 40 years ago. Since its invention, great efforts have been made to predict the melt front of capillary-driven underfill. The Hele-Shaw model, which calculates the behavior of fluids between two flat plates [1], was announced following Washburn's model for capillary flow in 1921 [2]. Several analytical models have been derived from these models, taking into account geometrical, tribological, and rheological variables.

Wan et al. proposed an analytical model in 2005 [3] that considers non-Newtonian fluid properties, successfully predicting the evolution of flow front and filling time of capillary encapsulation with solder bump effect. In 2007, they also established a model using the concept of a critical clearance [4], which deals with the filling time rapidly increasing below a certain value, aiming to find the optimal bump density. Yong developed a model in 2010 that incorporated both shear thinning and thickening behaviors based on temperature and filler concentration [5], advancing the prediction of filling time through rheological changes. Luo et al. developed a model considering various contact angles for each surface material of the flip-chip package that comes into contact with the encapsulant [6], allowing for a more accurate simulation of the capillary effect. Yao et al. [7] emphasized the implementation of solder bump arrangement in the analytical model by considering tortuosity in underfill flow prediction.

Using the aforementioned analytical models, predicting the melt front can be concisely and efficiently performed using variables that represent various mechanisms already established by previous researchers. However, as solder bump arrangements become more complex and the gaps become narrower with the evolution of devices, it becomes challenging to reflect the flow resistance. Additionally, the analytical model cannot account for the formation of voids due to the interaction between the contact line and geometrical heterogeneities [8]–[10]. The presence of voids in underfill encapsulation causes stress concentration in the flip-chip package, leading to reliability issues [11]. Thus,

addressing void issues is as crucial as enhancing productivity through filling time optimization. As a result, research groups have conducted 3D predictions using numerical analysis techniques to cover void-related concerns [12]–[19]. For 3D capillary driven underfill simulation studies, fluid dynamics software based on the Finite Volume Method (FVM) is commonly used. FVM-based studies have successfully simulated the relative difference in interfacial movement rate of the melting front due to the local difference in solder bump density, leading to macro void generation [12]–[16]. However, it becomes challenging to simulate micro-voids in systems where the characteristic length is less than 100um using FVM based on the continuum assumption. In such cases, properly reflecting the geometrical effect is difficult, and the resistance due to the solder array is converted into an equivalent model and reflected in the simulation, allowing only the analysis of filling time [17]–[19].

Recently, the lattice Boltzmann method (LBM) has been employed to simulate micro voids in underfill encapsulation. LBM implements molecular-level collision and stream statistics to micro-scale particles using distribution functions, enabling the simulation of phenomena occurring at interfaces between heterogeneous components, which are not considered in continuum-based models. Abas et al. conducted several numerical simulations of encapsulation on a 3D stacked chip package and a single-stage BGA package using LBM, confirming the occurrence of micro voids [20]–[22]. However, the packages analyzed in the mentioned LBM studies were composed of wire bonding without solder bumps or solder bumps of several millimeters, thus not at an industry-applicable level.

In this study, underfill simulation was performed under conditions involving solder bump arrangements and gap heights with a micro-scale characteristic length commonly used in the current semiconductor packaging field. LBM was utilized as the simulation method, and this LBM model improved the calculation ability of contact line friction and pressure in microbubbles based on previous studies [23], [24]. The differences in void generation behavior according to the bump pitch were observed, and the causes were identified based on the differences in the contact line movement mechanism according to the pitch. Additionally, the study revealed variations in the amount of void generated according to the ambient air pressure, and the reasons for these changes were derived through the analysis of the pressure field around the contact line, merging again after passing the solder bump.

II. Numerical Method

In this section, the LBM used in this study will be described. Based on the partial wetting model of Yan et al. [25], the authors of this paper improved the surface-wettability-implementation formula through prior research, and observed behavior of liquid droplets on surfaces with a wettability gradient using this formula [26]. For the main equations of the simulation model, please refer to previous research papers. In this study, the model was improved by adding contact-line friction, and the process is as follows.

Carlson et al. proposed an equation expressing the relationship between free energy change and interfacial phase gradient in dynamic wetting as follows [27].

$$\delta_\Gamma F = \int_\Gamma [\sigma\epsilon \nabla C \cdot \mathbf{n} + (\sigma_{sg} - \sigma_{sl}) w'(c)] \delta C d\Gamma \quad (1)$$

Where σ is a surface tension, ε is a thickness of the interface, C is a phase index, $\mathbf{n}$ is a unit normal vector of surface, w is a normalized and modeled density profile of interface, and Γ is a surface integral. Since the right side of the above equation is not 0 when a contact line is not in equilibrium, it can be expressed as an amount of deviation over time of the phase as shown in an equation below.

$$D_w^* \frac{\partial C}{\partial t} = \sigma\epsilon \nabla C \cdot \mathbf{n} + (\sigma_{sg} - \sigma_{sl}) w'(C), \quad (2)$$

Carlson et al. left D_w as an arbitrary value. In subsequent studies, assumptions have been made as necessary so that D_w can be transformed and utilized. In the follow-up study, the equation was constructed by replacing D_w with a friction factor μ_f as shown below [28].

$$\varepsilon\mu_f \frac{\partial C}{\partial t} = \varepsilon\sigma\nabla C \cdot n + \sigma\cos(\theta_e) w'(C) \quad (3)$$

The above equation is modified by confirming that the droplet-spreading-radius value can be normalized through a constant. Here, the friction factor is a constant that controls dissipation due to friction occurring in the contact line. In addition to viscous dissipations due to wedge flow and precursor-film generation, a third dissipation was predicted through an establishment of a theory on an interfacial dissipation through molecular kinetic theory (MKT) [29], and its existence has been proven through subsequent studies. It is named contact-line friction [28].

If (3) is summarized as (4) and $\sigma\cos(\theta_e)w'(C)/\varepsilon$ is changed to a wetting potential (λ) of the partial wetting model of LBM, it can be expressed as (5).

$$\mu_f \frac{\partial C}{\partial t} = \sigma\nabla C \cdot n + \sigma\cos(\theta_e) w'(C)/\varepsilon \quad (4)$$

$$\sigma\nabla C \cdot n = \mu_f \frac{\partial C}{\partial t} + \sigma\frac{\lambda}{k} \quad (5)$$

The ∇C value is used to implement a wettability and a contact-line friction on the LBM by replacing the phase

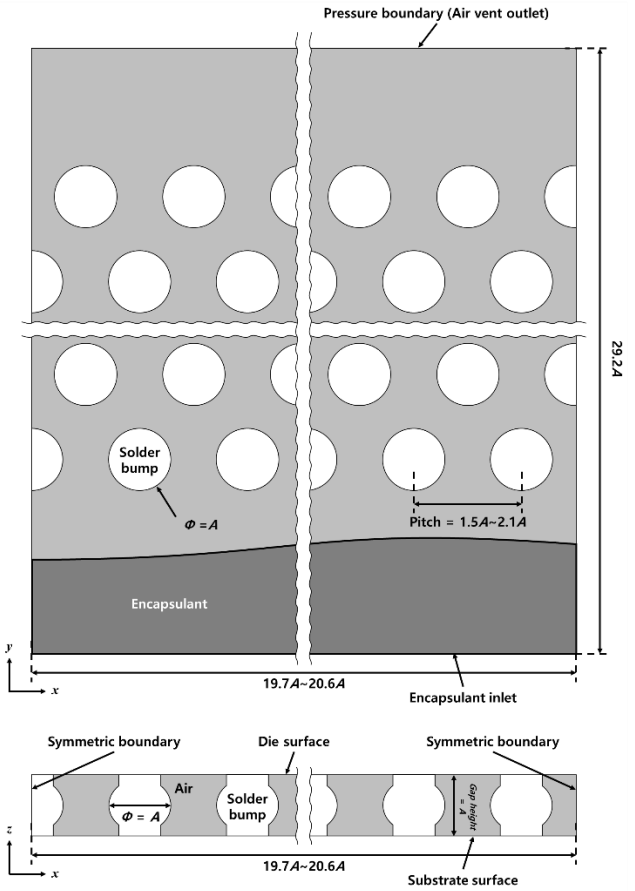

Fig. 1. A schematic diagram of a numerical analysis domain including encapsulant and solder bumps.

gradient value of the partial wetting model. Details about the contact-line-friction coefficient can be found in the author's previous research on a contact-line friction [23].

III. Results and Discussion

A. Simulation Domain Configuration

In the flip-chip package structure, the space between the die and the substrate is used as the analysis domain, configured in a situation where only the solder bump array exists before the encapsulant is filled. If A is the width of the solder bump in the simulation domain shown in Fig. 1, among the dimensions of the empty space to be filled with encapsulant, x varies from 19.7A to 20.6A depending on simulation cases, and y and z are fixed at 29.2A and 1.0A. The overall arrangement of the solder bump array is configured so that two adjacent solder ball lines in the y direction are staggered, and the pitch of the solder bump varies from 1.5A to 2.1A for each simulation case. Encapsulant penetrates into the space from the y = 0 boundary by the capillary effect, and the contact angles of each solid surface that creates a capillary are 35.0˚ on both of the die and substrate surfaces, and 20.0˚ on the solder bump surface. A symmetry condition is applied to x = 0 and the opposite boundary. A pressure condition is applied to the y = 29.2A boundary, and the pressure varies from 0.1 to 1.0 atm depending on the cases.

Most previous studies that performed 3D fluid dynamics analysis of underfill encapsulation included both the center area with solder bump array and the edge area without solder

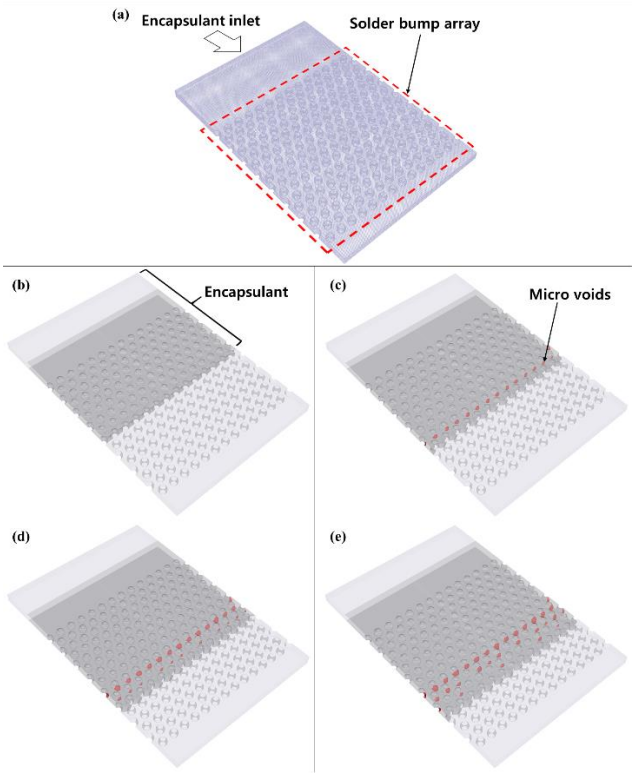

Fig. 2. Example of actual simulation results. (a) is the actual numerical analysis domain shape, and the solder bump pitch in this figure is 1.5A. Simulation time elapses from (b) to (e), micro voids are colored in red, and encapsulant flows are colored in gray.

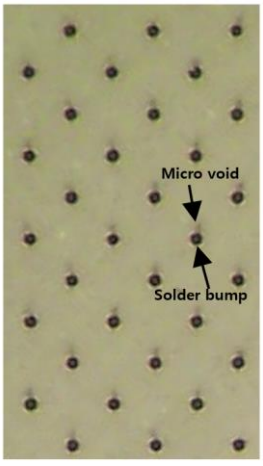

Fig. 3. Occurrence of micro voids confirmed through underfill process experiments. The black circular dots are solder bumps, and the translucent gray areas attached to the bumps are voids.

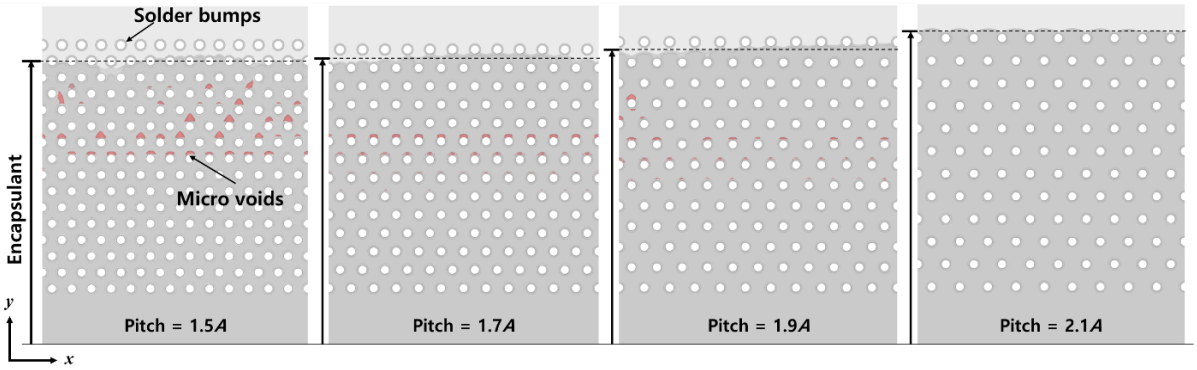

Fig. 4. Simulation results of encapsulant flow and void formation at bump pitch = 1.5*A*, 1.7*A*, 1.9*A*, and 2.1*A* respectively. All four figures are snapshots of the same point in time. The dotted line is the average position of the melting front in the *x* direction, and the void is marked in red.

bumps in the analysis domain [12]. The focus was placed on the contact line speed difference due to the difference in flow resistance in these two areas and macro void simulation resulting from this speed difference. On the other hand, as shown in Fig. 1, in this study, there is no edge area without solder bumps except for the underfill inlet and the outlet for air vent. This domain configuration allows focusing on the micro void formation process around the solder bump according to the bump pitch.

B. The Effect of Solder Bump Pitch on Micro Void Generation

It is widely recognized that the solder bump within the capillary underfill serves as a resistor impeding interface movement. The encapsulant receives capillary force from various surfaces - substrate, chip, and solder bump. However, the presence of the solder bump alters the trajectory of the encapsulant interface, compelling it to veer away from the solder bump while advancing. This deviation necessitates additional kinetic energy, consequently slowing down the interface motion. This section explores several scenarios involving different solder bump pitches to investigate their influence on micro void formation.

Fig. 2 illustrates the simulation domain shape utilized in this study and the simulation depicting the penetration of the encapsulant over time for a bump pitch of 1.5*A*. As the encapsulant's interface (melting front) advances, it fails to cover some part of the solder bump surface, leading to the formation of micro voids during the simulation. This phenomenon can also be confirmed through experiments. Fig. 3 is the result of underfill encapsulation performed by attaching solder bumps to glass. Since the glass is transparent, the interface shape of the encapsulant filled inside is observed. It is confirmed that micro voids are formed in front of each solder bump based on the melting front direction. This issue arises from insufficient smooth evacuation of air trapped between the chip and substrate as the melting front progresses. Analysis confirms that inadequate air release could be attributed to narrow gap height and bump pitch, leading to localized air pressure accumulation as the melting front advances. The air pressure surpasses a critical value, preventing the melting front from adequately enveloping the bump, leading to void formation. In Fig. 2, the air pressure crosses the threshold in the 9th row of bumps, initiating void formation from the 9th row onwards. The subsequent case study examines how solder bump arrangement affects air pressure near the melting front. Fig. 4 displays the bump pitch for each simulation case and the corresponding micro voids. A larger pitch of the solder

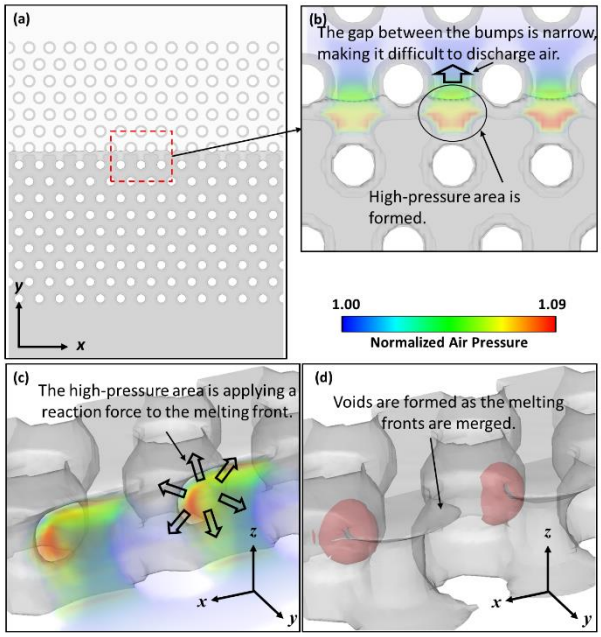

Fig. 5. Void formation process at pitch = 1.5*A*. (a) is the shape of the encapsulant and solder bump being advanced at a specific point in time, and (b) is an enlarged display of the red dotted line area. (b) shows the shape of the melting front and the surrounding air pressure contour. (c) shows the area shown in (b) from a different angle, and the air pressure around the melting front is displayed as a volume rendering. (d) shows the melting front shape at a later point than (b) or (c), and voids are marked in red.

bump results in increased advancement distance of the melting front along the *y*-direction. This hindrance caused by the solder bump on the encapsulant's progress has been previously established by other studies. Additionally, smaller pitches introduce greater irregularities in the *x*-direction of the melting front, correlating with a higher tendency for void generation. Smaller pitches exhibit more voids due to the shifting merge positions of the interfaces after the melting front bypasses the solder bumps. This phenomenon accumulates over successive rows of bumps, distorting the shape of the melting front. Notably, at a pitch of 2.1*A*, void generation is absent, and the melting front retains a horizontal shape.

Further insight into the varying void generation probabilities with respect to pitch involves analyzing the behavior of the melting front and air around the solder bump in extreme cases (pitch = 1.5*A* and 2.1*A*). Fig. 5 and 6 depict the melting front shape and localized air pressure contour at pitch values of 1.5*A* and 2.1*A*, respectively. Comparison of Fig. 5(b) with Fig. 6(b) reveals that a high-pressure zone forms in the vicinity where melting fronts converge at a pitch of 1.5*A*. This arises from the dominance of skin friction effects on air flow due to the small pitch, hindering air exhaust. As depicted in Fig. 5(c), the melting front assumes a ring-like

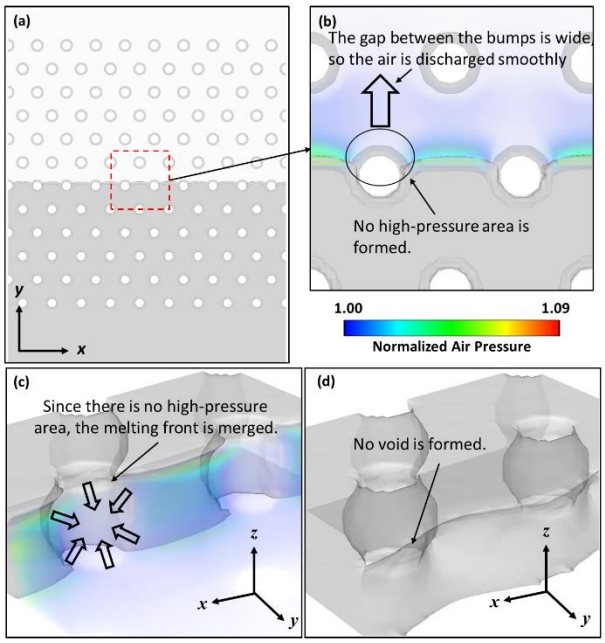

Fig. 6. Simulation result of encapsulant behavior at pitch = 2.1*A*. (a) is the shape of the encapsulant and solder bump being advanced at a specific point in time, and (b) is an enlarged display of the red dotted line area. (b) shows the shape of the melting front and the surrounding air pressure contour. (c) shows the area shown in (b) from a different angle, and the air pressure around the melting front is displayed as a volume rendering. (d) shows the melting front shape at a point later than (b) or (c), and voids are not formed, so they are not displayed.

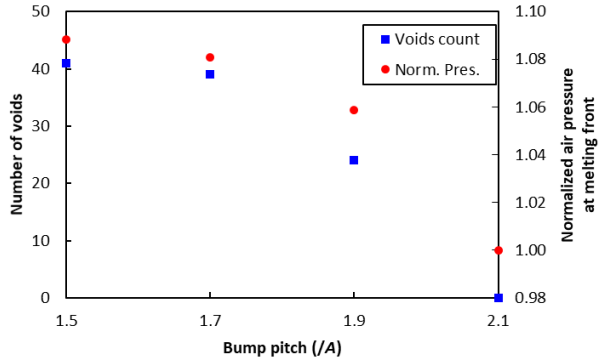

Fig. 7. The total number of voids of bump pitch = 1.5A, 1.7A, 1.9A and 2.1A, and the pressure around the melting front just before the first void is created.

shape on the solder bump's surface, with the high-pressure area exerting a repulsive force on the entire melting front ring.

Consequently, as shown in Fig. 5(d), the melting front merges at a distance from the bump's surface, trapping air between the bump and encapsulant. This distortion in melting front behavior becomes evident after the air pressure has sufficiently built up following the melting front's advancement. And Fig. 7 is a graph showing the pressure around the melting front just before the first void is created in each case, from this figure, it can be seen that the magnitude of the pressure built-up around the melting front is related to the total number of voids. Hence, as shown in Fig. 4, voids appear after the 9th row at pitch = 1.5*A* and after the 6th row at pitches of 1.7*A* and 1.9*A*. Conversely, at pitch = 2.1*A* as shown in Fig. 6(c), no high-pressure area forms around the melting front ring, facilitating smooth collapse of the ring and preventing void formation.

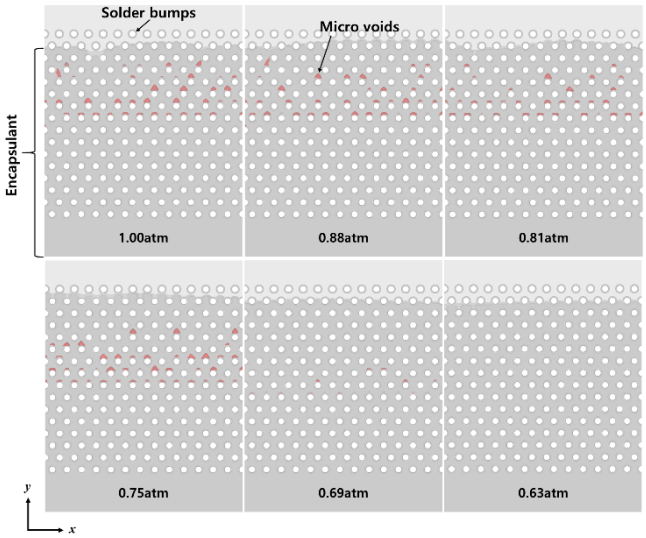

Fig. 8. Underfill simulation results according to air pressure. Encapsulants are shown in gray and voids in red. Pitch is 1.5*A*.

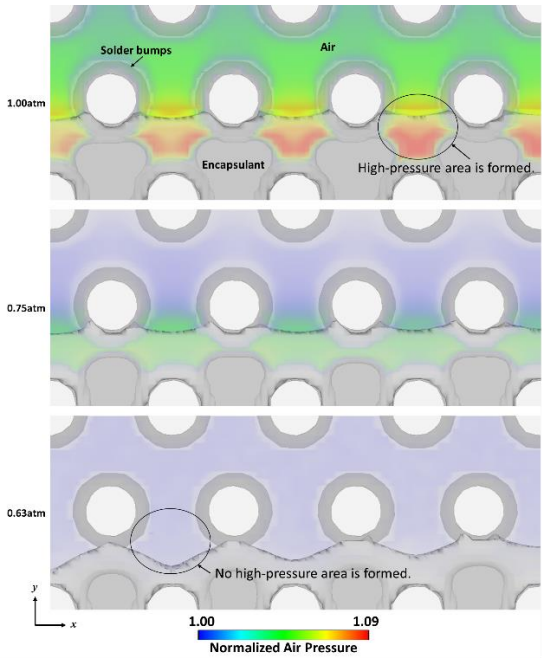

Fig. 9. Shapes of the melting front and ambient air pressure at pressures = 1.00, 0.75 and 0.63 atm. Air pressure is shown through volume rendering. Pitch is 1.5*A*.

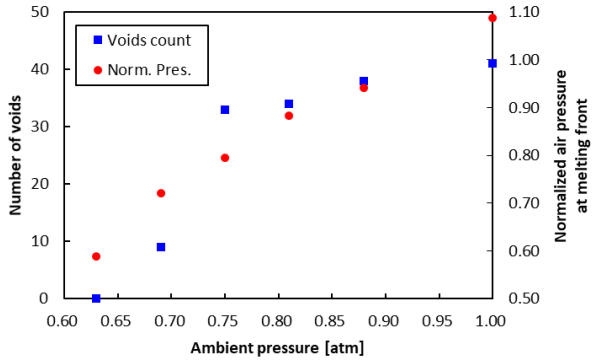

Fig. 10. The total number of voids generated depending on the ambient pressure, and the pressure around the melting front just before the first void is created. Pitch is 1.5*A*.

C. The Effect of Ambient Air Pressure

Variations exist in the capillary underfill process, including a technique that lowers the surrounding air pressure to minimize air resistance and enhance filling rate. This section investigates whether altering air pressure introduces any side effects related to void formation. Fig. 8 presents simulation results of the underfill process under different surrounding air pressures (ranging from 0.63 to 1.00 atm). Voids show no consistent change within the range of 0.75 to 1.00 atm. At 0.69 atm, fewer voids are notably present, and no voids emerge below 0.63 atm. Fig. 9 indicates that lower surrounding air pressure leads to reduced viscous dissipation and local pressure build-up, enabling smooth collapse of the melting front around the bump and preventing void formation. Summarizing the results of Fig. 8 and 9, there appears to be a critical pressure threshold that facilitates air ventilation, impacting void creation tendencies and the pressure build-up around the melting front.

In Figs. 7 and 10, the relationship between the pressure surrounding the melting front and the total number of voids is different. In the context of the bump pitch case study, a melting front pressure of 1.00 (pitch = 2.1*A*) correspond to zero voids. However, with a fixed pitch of 1.5*A* and varying ambient pressures, a melting front pressure of 0.80 or higher result in over 30 voids, while the number decrease to less than 10 for pressures below 0.72. This distinctive behavior appears to be attributed to the pitch factor. Smaller pitches seem to hinder pressure relief, making void formation more likely even at lower melting front pressures.

IV. Conclusion

This study conducted an underfill analysis considering micro-scale characteristics of solder bump arrangement and gap height commonly employed in semiconductor packaging. The in-house developed LBM analysis technique simulated the behavior of the contact line between the encapsulant interface and the substrate.

The investigation revealed varying void generation tendencies based on bump pitch, attributed to distinct pressure build-up mechanisms. Smaller pitches led to increased advancement distance of the melting front and greater irregularities in its shape. Void generation tendencies were analyzed by studying the melting front and air behavior around the solder bump. High-pressure areas formed in cases of small pitch due to dominant skin friction effects hindering air flow. This led to distorted melting front behavior and trapped air, resulting in voids. Conversely, larger bump pitches allowed smoother air ventilation and melting front collapse, preventing void formation. Variations in void generation based on ambient air pressure were confirmed, with pressure analysis revealing critical points for enhanced air ventilation. The pressure drop exhibited no adverse impact on void formation tendencies.

The numerical model employed in this study incorporates the thixotropic effect of the encapsulant. However, the associated analysis was not conducted, thus preventing the assertion that this study comprehensively addresses all the effects of bump pitch on underfill flow. Furthermore, due to variations in the arrangement and dimensions of bump pitches for each product, substantial differences in underfill flow behavior are anticipated across products. This renders the application of the analysis from this study to other products challenging.

Despite the limitations identified in this analysis, the local analytical examination of micro-scale contact line

advancement between bumps and the macro-scale void analysis within a solder bump array with several millimeter pitches have been treated separately up to this point. Therefore, in this study, there is value in transcending these limitations of previous research by merging these approaches.

In scenarios where the ambient air pressure is reduced during the underfill process, concerns regarding void formation are alleviated. However, regulating air pressure becomes problematic when multiple products are sequentially encapsulated on a single wafer or panel to enhance productivity. In such instances, an analysis of micro flow resistance based on the bump arrangement, as conducted in this study, offers valuable insights for refining and supplementing the product's bump configuration.

References

[1] C. A. Hieber, and S. F. Shen "A finite-element/finite-difference simulation of the injection-molding filling process," *J. Nonnewton Fluid Mech.*, vol. 7, 1980, pp. 1–32.

[2] E. W. Washburn, "The dynamics of capillary flow," *Phys. Rev.*, vol. 17, Mar. 1921, pp. 273–283.

[3] J. W. Wan, W. J. Zhang, and D. J. Bergstrom, "An analytical model for predicting the underfill flow characteristics in flip-chip encapsulation," *IEEE Trans. Adv. Packag.*, vol. 28, Aug. 2005, pp. 481–487.

[4] J. W. Wan, W. J. Zhang, and D. J. Bergstrom, "A theoretical analysis of the concept of critical clearance toward a design methodology for the flip-chip package," *J. Electron. Packag.*, vol. 129, Dec. 2007, pp. 473–478.

[5] W. Young, "Modeling of a non-Newtonian flow between parallel plates in a flip chip encapsulation," *Microelectron. Reliab.*, vol. 50, Jul. 2010, pp. 995–999.

[6] W. Luo, J. Liang, Y. Zhang, and H. Zhou, "An analytical model for the underfill flow driven by capillary forces in chip packaging," *2016 17th International Conference on Electronic Packaging Technology (ICEPT). IEEE*, Aug. 2016 pp. 1381–1386.

[7] X. j. Yao and W. J. Zhang, "An analytical model for permeability of underfill flow in flip-chip packaging with consideration of the actual specific surface and tortuosity," *IEEE Trans. Compon. Packag. Manuf.*, vol. 8, Aug. 2018, pp. 1507–1514.

[8] J. Wang, "The effects of rheological and wetting properties on underfill filler settling and flow voids in flip chip packages," *Microelectron. Reliab.*, vol. 47, Dec. 2007, pp. 1958–1966.

[9] M. Shih, and W. Young, "Experimental study of filling behaviors in the underfill encapsulation of a flip-chip," *Microelectron. Reliab.*, vol. 49, Dec. 2009, pp. 1555–1562.

[10] A. Abas, F. C. NG, Z. L. Gan, M. H. H. Ishak, M. Z. Abdullah, and G. Y. Chong, "Effect of scale size, orientation type and dispensing method on void formation in the CUF encapsulation of BGA," *Sādhanā*, vol. 43, Apr. 2018, pp. 1–14.

[11] P. S. Ho, Z. P. Xiong, and K, H, Chua, "Study on factors affecting underfill flow and underfill voids in a large-die flip chip ball grid array (FCBGA) package," *2007 9th Electronics Packaging Technology Conference. IEEE*, Dec. 2007, pp. 640–645.

[12] C. Y. Khor, M. Abdul Mujeebu, M. Z. Abdullah, and F. Che Ani, "Finite volume based CFD simulation of pressurized flip-chip underfill encapsulation process," *Microelectron. Reliab.*, vol. 50, Jan. 2010, pp. 98–105.

[13] C. Y. Khor, M. Z. Abdullah, M. Abdul Mujeebu, and F. Che Ani, "FVM based numerical study on the effect of solder bump arrangement on capillary driven flip chip underfill process," *Int. Commun. Heat Mass Transf.*, vol. 37, Mar. 2010, pp. 281–286.

[14] Ernest E. S. Ong, M. Z. Abdullah, C. Y. Khor, W. C. Leong, W. K. Loh, C. K. Ooi, and R. Chan, "Numerical modeling and analysis of microbump pitch effect in 3d IC package with TSV during molded underfill (MUF)," *Eng. Appl. Comput. Fluid Mech.*, vol. 7, 2013, pp. 210–222.

[15] K. B. Ham, J. Son, H. Im, and Y. Park, "Analysis of underfill process on micro-pitch flip-chip by epoxy filling rate," *J. Korean Soc. Precis. Eng.*, vol. 35, Jun. 2018 pp. 641–647.

[16] M. N. Nashrudin, A. Abas, M. Z. Abdullah, M. Y. T. Ali, Z. Samsudin, and I. Mansor, "No-flow underfill: Effect of chip placement speed on the void formation using numerical method," *Microelectron. J.*, vol. 114, Aug. 2021, p. 105139.

[17] C. Y. Khor, M. Z. Abdullah, and M. Abdul Mujeebu, "Influence of gap height in flip chip underfill process with non-Newtonian flow between two parallel plates," *J. Electron. Packag.*, vol. 134, Mar. 2012, p. 011003.

[18] C. Yang, and W. Young, "The effective permeability of the underfill flow domain in flip-chip packaging," *Appl. Math. Model.*, vol. 37, Feb. 2013, pp.1177–1186.

[19] Y. E. Liang, C. P. Sun, C. C. Hsu, D. C. Hu, E. H. Chen, and J. C. Lee, "A novel equivalent model for underfill molding process on 2.2D structure for high performance applications," *2022 IEEE 72nd Electronic Components and Technology Conference (ECTC). IEEE*, May. 2022, pp. 531–538.

[20] A. Abas, Z. L. Gan, M. H. H. Ishak, M. Z. Abdullah, and S. F. Khor, "Lattice Boltzmann method of different BGA orientations on I-type dispensing method," *PloS one*, Jul. 2016, p. e0159357.

[21] M. H. H. Ishak, M. Z. Abdullah, and A. Abas, "Lattice Boltzmann method study of effect three dimensional stacking-chip package layout on micro-void formation during encapsulation process," *Microelectron. Reliab.*, vol. 65, Oct. 2016, pp. 205–216.

[22] Z. L. Gan, A. Abas, M. H. H. Ishak, and N. J. Loung, "Lattice-Boltzmann analysis of pressurized underfill process for I-type dispensing method," *AIP Conf. Proc. International Conference on Mathematics, Engineering and Industrial Applications 2016*, vol. 1775, Oct. 2016, p. 030091.

[23] H. M. Yoon, S. Kondaraju, J. S. Lee, Y. Suh, J. H. Lee, and J. S. Lee, "Molecular dynamics study of the nanosized droplet spreading: The effect of the contact line forces on the kinetic energy dissipation," *Appl. Surf. Sci.*, vol. 409, Jul. 2017, pp. 179–186.

[24] J. S. Lee, J. W. Cho, S. W. Park, S. Lee, H. Lee, and D. M. W. Rhee, "Direct patterning of conductive fine line in dielectric layer for semiconductor package," *2020 IEEE 22nd Electronics Packaging Technology Conference (EPTC). IEEE*, Dec. 2020, pp. 472–478.

[25] Y. Y. Yan, and Y. Q. Zu, "A lattice Boltzmann method for incompressible two-phase flows on partial wetting surface with large density ratio," *J. Comput. Phys.*, vol. 227, Nov. 2007, pp. 763–775.

[26] J. S. Lee, J. Y. Moon, and J. S. Lee, "Study of transporting of droplets on heterogeneous surface structure using the lattice Boltzmann approach," *Appl. Therm. Eng.*, vol. 72, Nov. 2014, pp. 104–113.

[27] A. Carlson, M. Do-Quang, and G. Amberg, "Modeling of dynamic wetting far from equilibrium," *Phys. Fluids*, vol. 21, Dec. 2009, p. 121701.

[28] A. Carlson, G. Bellani, and G. Amberg, "Universality in dynamic wetting dominated by contact-line friction," *Phys. Rev. E*, vol. 85, Apr. 2012, p. 045302.

[29] D. Seveno, N. Dinter, and J. De Coninck, "Wetting dynamics of drop spreading. New evidence for the microscopic validity of the molecular-kinetic theory," *Langmuir*, vol. 26, Aug. 2010, pp. 14642–14647.